Further Development of Sheet Metal Forming Analysis Method

S. A. Majlessi

D. Lee

Department of Mechanical Engineering, Aeronautical Engineering and Mechanics, Rensselaer Polytechnic Institute, Troy, New York 12181

The finite element analysis procedure used to model the sheet metal forming process is further developed by incorporating a refined numerical procedure and an improved metal-tool friction analysis method. The shell-type model is capable of closely approximating the strain distribution of prescribed axisymmetric parts. Further refinements on the numerical procedure have resulted in the marked decrease of the time required to reach a convergence of solutions. At the same time, frictional conditions at the metal-die and metal-punch interfaces have been closely characterized by applying equilibrium conditions in an iterative manner. Effects of these improved procedures have been examined in detail by making a systematic sensitivity analysis and by comparing the analytical results against experimental data. Based on these results, a critical assessment of the simplified analysis method is made.

1 Introduction

The computer simulation of complex manufacturing problems has the advantage of enabling the engineer to modify the design in the blue-print stage. Material deformation processes, due to their inherent complexity and large number of controlling variables, are ideally suited for these types of applications. This is especially true for deformation processing operations such as sheet metal forming, where a considerable portion of material can be easily wasted when the conventional trial-and-error procedure is used during the prototyping process.

Deep drawing, which is a widely used sheet metal processing method, is frequently utilized as a means of examining the drawability of sheet materials. A number of investigators have studied the drawing process to obtain analytical and numerical solutions. One of the first successful analytical attempts was made by Chung and Swift [1] who developed a method of analyzing the radial drawing process. It was assumed, among other things, that the numerical value of the equivalent strain is equal to that of the circumferential strain. This assumption was shown to be true for the plane drawing in the flange region by Hill [2], and later by Woo [4]. Extensive work was done by Woo, who developed a method for analyzing the axisymmetric forming process based on the general theories of rigid-plastic material model and equilibrium equations, and the analysis was applied to hydrostatic bulging [3], stretch forming [4], and deep drawing processes [5, 6]. Yamada [7] employed both total and incremental strain theories of plasticity in the analysis and predicted the punch force for the radial drawing of an isotropic material. Budiansky and Wang [8] used a rigid-plastic orthotropic material model and utilized a finite deformation theory to analyze a cup drawing process.

Availability of high-speed computers motivated a number of investigators to analyze the sheet metal forming process with the finite element method. Most of these efforts were concerned with the analysis of the axisymmetric problem using a rigid-plastic material model and the incremental theory of plasticity [9, 10]. The process of nonaxisymmetric sheet metal forming has also been examined by several researchers. Toh and Kobayashi [11–13] modeled this process using a rigid-plastic finite element analysis method based on membrane theory, and analyzed deep drawing of nonaxisymmetric geometries. Kim and Yang [14] also developed a general incremental rigid-plastic finite element analysis formulation of large strains, and analyzed hydrostatic bulging of circular and rectangular sheet materials.

When large deformation problems are examined, the results of the finite element analysis method based on the rigid-plastic formulation are in good agreement with experimental observations. Nevertheless, the method does not account for the elastic unloading, and therefore, such phenomena as springback and development of residual stresses cannot be handled by the model. Development of the elasto-plastic finite element analyses has been accomplished partially on that account. Wifi [15] formulated an incremental variational method to analyze axisymmetric elastic-plastic solids, and applied the analysis to solve deep drawing of circular blanks. In a later study, the stamping process of an elastic-plastic sheet material was examined by Wang and Budiansky [16], where the effects associated with finite deformation and normal anisotropy were considered. As an alternative approach, Levy et al. applied the deformation theory of plasticity to approximate a cup-drawing analysis of an elastic-plastic material, and it was shown that considerable savings in computational time was achieved by using the deformation theory [17].

Other numerical techniques have also been used to model sheet metal forming processes. Kaftanoglu and Tekkaya [18] presented a finite difference method for analyzing the deep drawing process. Gerdeen and coworkers [19, 20] developed a "geometrical mapping" process in which the final configuration of the part was mapped onto the initial blank sheet by assuming the areas of a finite number of surface elements remained constant during deformation.

Contributed by the Production Engineering Division for publication in the JOURNAL OF ENGINEERING FOR INDUSTRY. Manuscript received at ASME Headquarters, May 15, 1987.

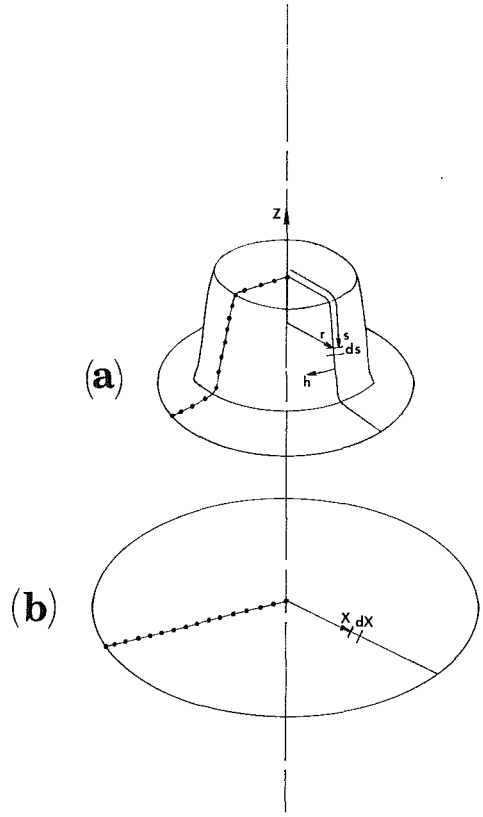

Fig. 1 Geometry of the problem, the associated coordinate system, and the nodal points along the meridian line in (a) deformed configuration, (b) initial flat sheet

Although a number of general purpose, finite element codes have been developed lately for analyzing nonlinear problems [21–23], they are not suitable for analyzing sheet metal forming processes. Moreover, the prohibitive length of computation time has prevented the use of such programs as an interactive tool at the design stage. The advantage of the use of membrane type elements and deformation theory of plasticity is the simplicity. With such a simplified method, solutions may be obtained quickly, and they are yet within an acceptable range of engineering approximations. In the present work, an improved numerical scheme is incorporated in which an elastic stress-strain relationship is used to initiate the solution. The converged solutions, which contain information about the history of deformation, are used as starting points to initiate the actual solution schemes. Furthermore, the frictional forces at the metal-tool interfaces are determined by considering the equilibrium of forces and are updated in each iteration until a satisfactory convergence is achieved.

2 Analytical Background

2.1 Description of the Simplified Finite Element Method. The analytical basis for the simplified finite element analysis of the axisymmetric sheet metal forming process was described by Levy et al. [17]. It was assumed that the part is deformed from the blank sheet to its final shape in a single step. Lee and coworkers [24–26] have further developed procedures for predicting the success or failure of the particular sheet metal design by incorporating a modified strain analysis method.

The symmetry condition in an axisymmetric part requires that the strain analysis be made only along a meridian line. Therefore, the analysis is carried out by dividing the meridian of the formed part into a finite number of one-dimensional curved elements. The coordinates of the nodes of elements

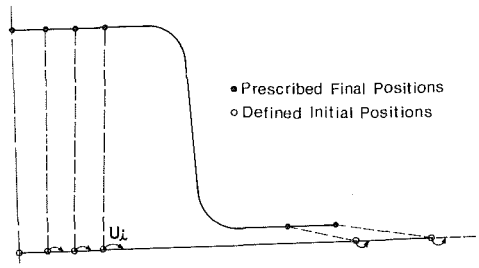

Fig. 2 Intial trial nodal locations on the blank sheet and their improved positions

along the meridian of the final geometry are defined as shown in Fig. 1(a). This approach is somewhat different from the conventional finite element method where the blank material is subjected to prescribed loading or displacement boundary conditions. In the present work, the geometry of the formed part and the initial sheet thickness are given, and the coordinates of elements are prescribed on the final shape. The unknowns are the initial locations of the nodes as well as the size of the initial blank sheet. These unknowns are determined by applying the principle of the minimum potential energy. Once the positions of the nodes on the undeformed sheet are determined, all the field variables can be calculated.

The following two assumptions have been made. First, the deformation (total strain) theory of plasticity is assumed to be applicable. This assumption is examined in detail in a separate paper [28], where the strain distributions are computed for an axisymmetric cup formed in several steps. It has been observed that the principal strain components are proportional for the material points located under the punch and in the flange regions. As the material points are drawn into the die and form the wall section of the cup, some nonproportionality of the strains is observed. In a study of sheet necking Hutchinson and Neale [29] compared predictions based on a total and incremental form of J_2 deformation theory and the J_2 flow theory. They concluded that where the forming histories do not deviate distinctly from proportional loading, a J_2 deformation theory is the better choice. Stören and Rice [30] have also analyzed sheet necking and reported good agreement between predictions based on the J_2 deformation theory and experimental observations. Second, the plane stress condition is assumed to be valid. The basis of the mathematical formulation is summarized in the following section.

The initial positions of all the nodes on the undeformed sheet, $\{X\}$, are first defined as shown in Fig. 1(b). These positions will be adjusted to $\{X+u\}$ in the course of numerical iteration. where $\{u\}$ denotes increments of small displacements of nodal positions (Fig. 2). Using the prescribed final location of nodes, $\{s\}$, logarithmic strains in the hoop and tangential directions are calculated. Therefore,

$$\epsilon = \epsilon(X, s) \tag{1}$$

The associated Cauchy stress, σ, can be determined by utilizing the material constitutive equation, $\bar{\sigma} = \bar{\sigma}(\bar{\epsilon})$, and the deformation theory of plasticity. Therefore,

$$\sigma = \sigma(X, s) \tag{2}$$

The potential energy, Ψ, is then calculated by:

$$\Psi = \int_V \left(\int_0^{\epsilon_f} \sigma \mathrm{d}\epsilon \right) \mathrm{d}V - \int_{S_r} T w \mathrm{d}S \tag{3}$$

where ϵ_f is final strain, T is surface tractions, w is boundary displacement, and S_r is the portion of the boundary where surface tractions are prescribed. The first term in equation (3) corresponds to the strain energy of deformation and the second term represents the work of external tractions. Any incremental changes in the location of the nodes in the undeformed state, $\{u\}$, will give rise to a change in the poten-

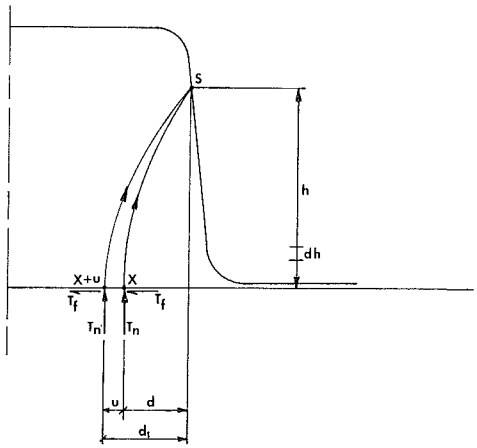

Fig. 3 Schematic presentation of the traction forces acting on a node before and after the improvement of the nodal position

tial energy. In particular, if the nodal positions are displaced to their correct position, $\{X+u\}$, the equilibrium equation will be satisfied and potential energy reaches a minimum value. Minimization of the potential energy is achieved by the following equation,

$$\frac{\partial \Psi}{\partial \{u\}} = 0 \tag{4}$$

where $\{u\}$ can be determined from the solution of equation (4). More specifically two quantities Ψ_X and Ψ_u can be defined in the following manner,

$$\Psi_X = \int_V \left(\int_0^{\epsilon_X} \sigma d\epsilon \right) dV - \int_{S_r} T_X w_X dS, \text{ and} \tag{5}$$

$$\Psi_u = \int_V \left(\int_{\epsilon_X}^{\epsilon_f} \sigma d\epsilon \right) dV - \int_{S_r} T_u w_u dS \tag{6}$$

where Ψ_X is the potential energy due to the deformation of the initially assumed (trial) nodal points to their final positions in the deformed configuration, and Ψ_u is the energy associated with the displacement of trial nodes to their modified locations in the undeformed geometry. The corresponding strain energy in equations (3), (5), and (6) are related by the following equation:

$$\int_0^{\epsilon_f} \sigma d\epsilon = \int_0^{\epsilon_X} \sigma d\epsilon + \int_{\epsilon_X}^{\epsilon_f} \sigma d\epsilon \tag{7}$$

Referring to Fig. 3, the work done by the normal component of traction T_n, when the material point located at X is deformed to s, is the same as the work done by T_n when the material point is initially at $(X+u)$ and has deformed to the same point s. The magnitude of this work is given by $W_n = \int_1 \vec{T}_n \cdot \vec{d1} = T_n \cdot h$, where 1 denotes the displacement from the undeformed to the deformed configuration. Work done by the frictional force T_f, due to the above two sets of displacements are not the same and differ by the quantity $(T_f \cdot u)$. This is due to the fact that $W_f = \int_1 \vec{T}_f \cdot \vec{d1} = T_f \cdot \mathbf{d}_1$, or $W_f = (T_f \cdot u) + (T_f \cdot \mathbf{d})$, where W_f is the frictional work due to deformation from $(X+u)$ to s. The sum of W_n and $(T_f \cdot \mathbf{d})$ constitutes the total work of tractions for the deformation from X to s, i.e., $\int_{S_r} T w_X dS$. Similarly $(T_f \cdot u)$ is the work of tractions along displacement u, $\int_{S_r} T w_u dS$. Therefore, the following equation can be written:

$$\int_{S_r} T w dS = \int_{S_r} T w_X dS + \int_{S_r} T w_u dS \tag{8}$$

The above equation was derived for the nodes located at the metal-punch interface shown in Fig. 3; the same relationship holds for the nodes at the metal-die interface. From equations (3) and (5)–(8), the potential energy can be decomposed into the two parts as follows,

$$\Psi = \Psi_X + \Psi_u \tag{9}$$

Since Ψ_X is constant with respect to $\{u\}$, equation (4) reduces to

$$\frac{\partial \Psi_u}{\partial \{u\}} = 0 \tag{10}$$

By expressing σ and ϵ as linear functions of displacement $\{u\}$, equation (10) yields a set of simultaneous linear equations in $\{u\}$. The $\{u\}$ values obtained from this set of equations are used to correct the position of the initial trial nodal points in the undeformed geometry to $\{X+u\}$. Due to the errors that may be introduced into the analysis by the linearization process, the correct displacements, $\{u\}$, have to be determined through an iteration procedure.

2.2 Description of the Enhanced Numerical Scheme. The iterative procedure of finding the correct set of values of $\{u\}$ utilizes a variant of the Newton-Raphson scheme. That scheme, however, has the inherent limitation of being too sensitive to the initial assumed solution. In the early version of the analysis, nodal locations on the undeformed sheet were selected by assuming $X_i = s_i \cdot$ scale, where s_i's are the prescribed positions of nodes on the deformed geometry and scale is an arbitrary factor which is less than unity. However, since initial $\{X\}$ values are selected arbitrarily the program may diverge; in which case a new set of initial $\{X\}$ values is defined and the process is started over again. The program has to search through $\{X\}$ values and carry out 10 to 50 iterations before a set of suitable $\{X\}$ values is obtained. The difficulty originates from the two sources of nonlinearities, i. e., the geometrical description and the stress-strain relationship. To overcome these difficulties, the following alternative scheme was employed. Initially, a completely elastic material which has the same Young's modulus as the actual material is assumed. The iterative scheme is initiated using the stress-strain relationship of the elastic material with any arbitrary trial nodal locations, $\{X\}$. The convergence is achieved quickly in about 5 iterations, resulting in u_i values $\leq 10^{-7}$ for the last iteration.

At the end of this cycle, the adjusted nodal values, $\{X+u\}$, correspond to the equilibrium positions which are associated with the assumed elastic material. These new nodal positions, which contain information about the specific history of deformation, constitute appropriate trial values for initiating the solution with the nonlinear material model. The rate of convergence is improved and values of u_i less than 10^{-7} are achieved within 5 to 10 iterations. Therefore, with the total number of iterations for elastic material and the real material model, a convergence is readily achieved and the lengthy search through $\{X\}$ domain is avoided. Moreover, the convergence is not sensitive to the assumed values of $\{X\}$ and any set of initial nodal points leads to a unique solution.

2.3 Description of Frictional Conditions. In sheet metal forming, most of the material is in continuous contact with the punch and dies during deformation. The role of friction on the deformation pattern and distribution of stresses and strains is especially important where the surface area to volume ratio is relatively large. Application of the total strain theory and hence disregarding the history of deformation prevents a rigorous modeling of the contact problem. Therefore, a simplified method of calculating frictional forces is developed which imposes the force equilibrium condition at the metal-tool interfaces.

2.3.1 Friction at Metal-Punch Interface From the

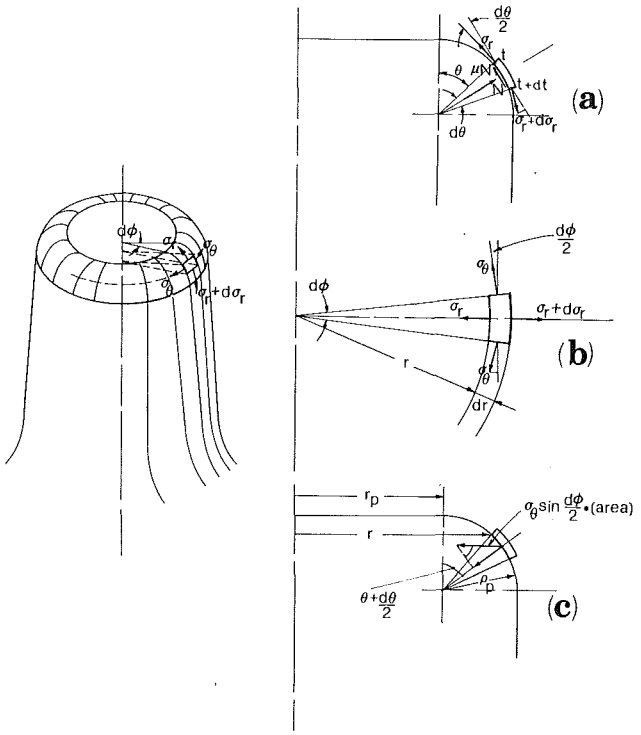

Fig. 4 Geometry and free body diagram of an infinitesimal element in the punch profile (a) side view, (b) top view, (c) side view

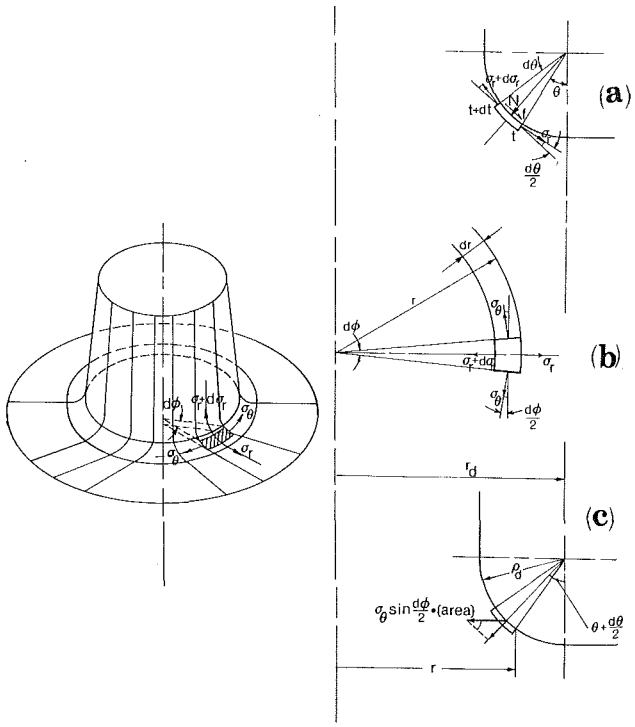

Fig. 5 Geometry and free body diagram of an infinitesimal element in the die profile (a) side view, (b) top view, (c) side view

physical description of the problem, it is concluded that frictional force is applied to the metal largely by the edge of the punch and not by its flat section. Therefore, it has been asumed that friction force is present wherever there is a curvature on the surface of the sheet. This argument is valid only for the case of relatively thin sheets.

Figure 4 shows an infinitesimal surface element of the sheet in the corner radius of the punch. Figures 4(a) and 4(b) show the free body diagram of a surface element. The equilibrium of forces in directions normal and tangential to the element are then considered. It should be noted that hoop stresses, which act on the lateral edges of the element, as shown in Fig. 4(b), are lying in the horizontal plane perpendicular to the axis of symmetry; therefore, their tangent components cancel out each other and leave only the normal components, σ_θ sin $d\phi/2$, to contribute to equilibrium [Fig. 4(c)]. Equilibrium of forces in the normal direction yields,

$$\rho_p N\mathbf{d}\theta(r+\mathbf{d}r/2)\mathbf{d}\phi - \sigma_r t r\mathbf{d}\phi \sin \mathbf{d}\theta/2 - (\sigma_r+\mathbf{d}\sigma_r)(t+\mathbf{d}t)(r+\mathbf{d}r)\mathbf{d}\phi \sin \mathbf{d}\theta/2 - 2\sigma_\theta\rho_p\mathbf{d}\theta \sin(\theta+\mathbf{d}\theta/2)(t+\mathbf{d}t/2)\sin \mathbf{d}\phi/2 = 0 \quad (11)$$

and in tangential direction,

$$\mu_p N\rho_p\mathbf{d}\theta(r+\mathbf{d}r/2)\mathbf{d}\phi + \sigma_r t r\mathbf{d}\phi \cos \mathbf{d}\theta/2 - (\sigma_r+\mathbf{d}\sigma_r)(t+\mathbf{d}t)(r+\mathbf{d}r)\mathbf{d}\phi \cos \mathbf{d}\theta/2 + 2\sigma_\theta\rho_p\mathbf{d}\theta \cos(\theta+\mathbf{d}\theta/2)(t+\mathbf{d}t/2)\sin \mathbf{d}\phi/2 = 0 \quad (12)$$

where N is normal reaction stress, μ_p is coefficient of friction at the metal-punch interface, t is current thickness, and ρ_p is the radius of the punch corner. Simplifying equation (11) and neglecting third order infinitesimal values, it yields,

$$\rho_p N r\mathbf{d}\phi\mathbf{d}\theta - \sigma_r t r\mathbf{d}\phi\mathbf{d}\theta - \sigma_\theta t\rho_p \sin\theta\mathbf{d}\theta\mathbf{d}\phi = 0 \quad (13)$$

Since $\sin\theta = r - r_p/\rho_p$ from Fig. 4(c), equation (13) reduces to,

$$f = \mu_p N = \frac{\mu_p t}{\rho_p}\left[\sigma_r + \sigma_\theta\left(1 - \frac{r_p}{r}\right)\right] \quad (14)$$

where r_p is the distance between the center of punch radius and the axis of symmetry. It should be noted that the quantity f in equation (14) has the dimension of force per unit area, representing the frictional shear stress. The corresponding frictional force per unit length of the line elements is numerically identical to f, provided that this force is considered for a unit width in the circumferential direction. This is equivalent to assuming that line elements have a width of unity. Frictional forces at each nodal point are then determined by the following relationship:

$$F_i = \int_S [N_i]^T \cdot f \cdot \mathbf{d}S = \int_{-1}^{1} [N_i(\xi)]^T \cdot f(\xi) \cdot \frac{\mathbf{d}S}{\mathbf{d}\xi} \cdot \mathbf{d}\xi \quad i = 1,2,3$$

where S is length of the line element, N shape functions, and ξ denotes the local coordinate system. The above integral is estimated by Gauss quadrature as,

$$F_i = \sum_{j=1}^{3} ([N_i]^T)_j \cdot f_j \cdot \left(\frac{\mathbf{d}S}{\mathbf{d}\xi}\right)_j \cdot w_j \quad i = 1,2,3$$

where w_j are weight functions and j refers to Gauss point.

2.3.2 Friction at Metal-Die Interface. In sheet metal forming, the blank holder pressure is an independent variable and is specified as an input. The reaction forces at the die surface, however, can be calculated using equilibrium equations in the same way as shown in section 2.3.1. Figure 5 shows an infinitesimal surface element of the material on the corner radius of the die. The free body diagram of this element is shown in Figs. 5(a) and 5(b). Hoop stress, σ_θ, is again lying in a horizontal plane and only its normal component, $\sigma_\theta \sin \mathbf{d}\phi/2$, contributes to equilibrium of forces [Fig. 5(c)]. In normal and tangential directions, equilibrium of forces yields exactly the same equations as equations (11) and (12), except that the sign of the last term in each equation is reversed and the subscripts p (for punch) are replaced by $\mathbf{d}$(for die). Then by defining $r_\mathbf{d}$ as shown in Fig. 5(c), $\sin\theta = r_\mathbf{d} - r/\rho_\mathbf{d}$. Substituting this relationship into the equilibrium equation in the normal direction gives,

$$f = \mu_\mathbf{d} N = \frac{\mu_\mathbf{d} t}{\rho_\mathbf{d}}\left[\sigma_r + \sigma_\theta\left(1 - \frac{r_\mathbf{d}}{\mathbf{r}}\right)\right] \quad (15)$$

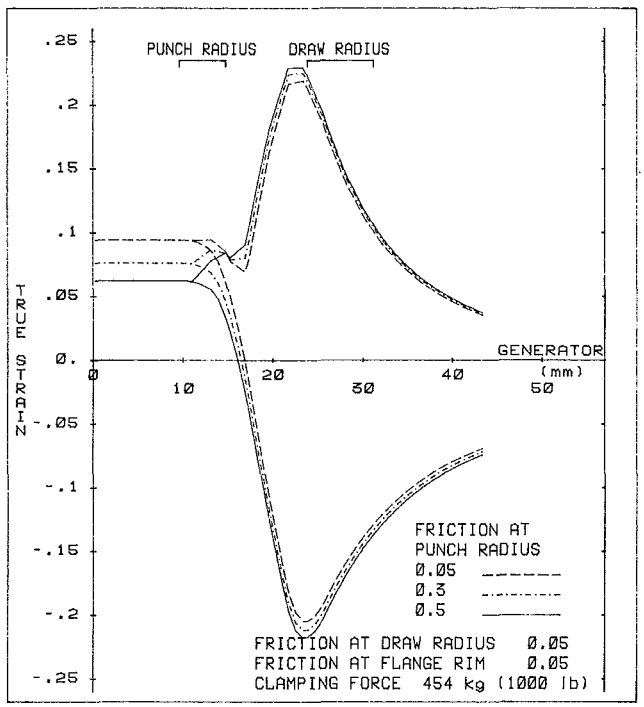

(a)

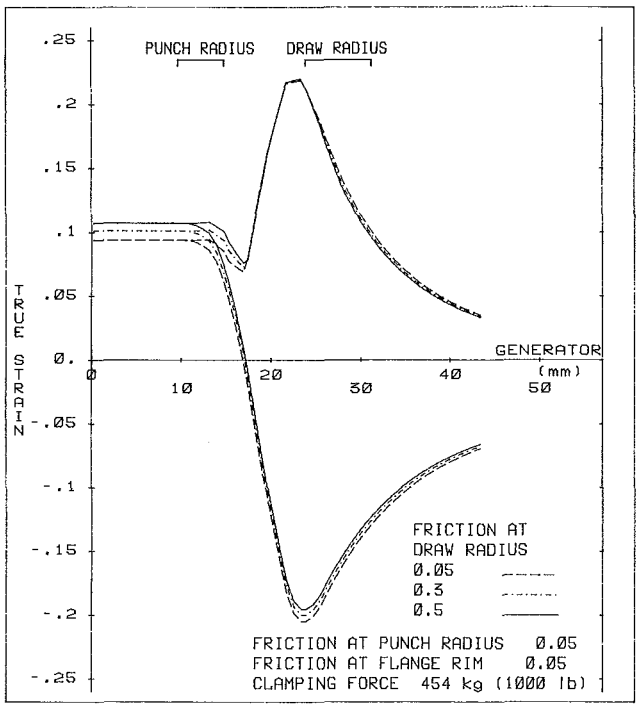

(b)

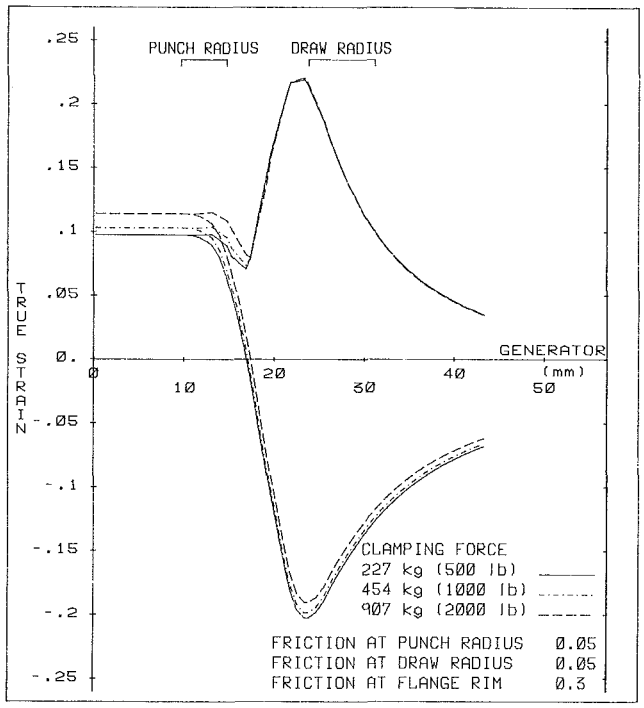

(c)

Fig. 6 Diagram showing effects of changing friction coefficient in the (a) punch profile and (b) die profile regions; (c) shows effect of changing clamping force at the flange rim. Data obtained for a 41-noded High Strength Steep cup model.

Note that equation (15) is similar to equation (14) of the previous section. Calculation of the equivalent nodal forces also follows the same method as previously described.

2.3.3 Friction at Metal-Blank Holder Interface. Due to the assumption of plane stress, the general practice of assigning frictional forces in the flange region is to concentrate all of the clamping force of the nodes located at the outer rim of flange [13]. This approach is reasonable because the flange region may become thicker during deformation with its thickest section being the outer rim of the flange. Experimentally, the bright edge of the flange section is observed after the cup is formed, indicating that higher normal and friction force are seen by the material at that location. The Coulomb frictional force is then calculated and is assigned to the outmost node on the flange.

It should be noted that directions of frictional forces are functions of the relative movement of the sheet metal with respect to the punch and die, and these directions are not known in advance. A brief description of an approach to determine these directions is given in the following section. The work of the friction over the displacement u is designated by W_f. Referring to Fig. 3, the following equation can be written

$$W_f = \vec{T}_f \cdot \vec{\mathbf{d}}_1 = -|T_f| \cdot |\mathbf{d}_1| \tag{16}$$

but for the case shown in Fig. 3, $|\mathbf{d}_1| = |u| + |\mathbf{d}|$. Therefore, $W_f = -|T_f| \cdot |u| - |T_f| \cdot |\mathbf{d}|$ where the first term in the above equation is the frictional work due to the increments of u. It can be shown that equation (10) may be written as,

$$\frac{\partial \Psi_s}{\partial \{u\}} - \frac{\partial}{\partial |u|} \cdot \frac{\partial |u|}{\partial \{u\}} \int_{S_r} -|T_f|\ |u|\ \mathbf{d}S = 0$$

where Ψ_s represents the strain energy, and $\partial |u| / \partial \{u\} = \pm 1$. Therefore,

$$\frac{\partial \Psi_s}{\partial \{u\}} \pm \frac{\partial}{\partial |u|} \int_{S_r} |T_f|\ |u|\ \mathbf{d}S = 0$$

Examination of various possibilities of relative positions of X, $X+u$, and s shows that the sign of the frictional force is the same as the sign of the vector $\mathbf{d}$. This feature has been accounted for in the program so that $\mathbf{d}$ for each nodal point i, is examined in each iteration and an appropriate sign for frictional force of that node is assigned.

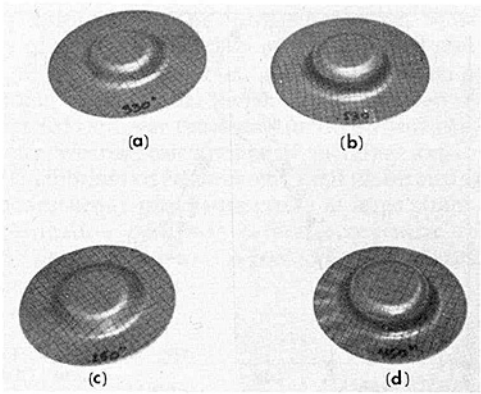

Fig. 7 Photographs of the EIDQ steel cup specimens formed under lubricated (top row) and dry (bottom row) conditions

3 Results and Discussion

3.1 Sensitivity of the Model to Friction. In order to identify the role of friction on the strain distribution, different friction coefficients have been assigned to punch, die, and blank holder areas. In the following cases, coefficient of friction at the flange rim was taken to be a constant value of 0.05 and variations of the frictional force at the rim were examined by changing clamp force. A 41-noded High Strength Steel cup model was first analyzed with friction varying at the punch radius only. The cup geometry is shown in the inset of Fig. 8(a) and the material parameters are summarized in Table 1.

As a reference condition, the friction coefficient at the punch and die profile regions was taken to be equal to 0.05, and the clamping force to be 454 kg (1000 lb). Coefficient of friction at the punch radius was then increased from 0.05 to 0.3, and 0.5. The strain distributions are depicted in Fig. 6(a). A considerable change of the strain distribution is observed in the flat as well as radius areas of the punch. By increasing friction of the punch region, the material lying on the punch is more constrained, and therefore deforms less. However, since the final configuration is fixed, the necessary deformation is provided by other portions of the cup, resulting in an increase of strain in the wall and flange regions.

Next, the friction coefficient at the die profile radius was increased from 0.05 to 0.3 and 0.5, while that of the punch profile and the clamping force were kept constant at 0.05 and 454 kg, respectively. The results are shown in Fig. 6(b). Friction in the die radius has caused strain components of the die area to decrease and those of the punch area increased.

Finally, the effect of frictional force in the flange rim was examined. Clamping forces of 227 kg (500 lb), 454 kg (1000 lb), and 907 kg (2000 lb) were applied, while friction coefficients at the punch and die regions were kept at 0.05. It was observed that when a low friction coefficient of 0.05 is used for flange rim, variations of clamping force do not affect the strain distribution. However, if a higher friction coefficient of 0.3 is used at the blank holder rim, an increase in the clamping force causes the hoop strain to decrease outside the punch area and both radial and hoop strain components to increase in the punch region as shown in Fig. 6(c).

3.2 Comparison of Analytical and Experimental Results. Two sets of axisymmetric cups were formed from Enameling Iron Drawing Quality (EIDQ) steel sheet with thickness of 0.69 mm (0.027 in.). The uniaxial test data of the sheet is assumed to follow the equation shown below [24].

$$\bar{\sigma} = K_0(\bar{\epsilon} + \epsilon_0)^n \cdot \left[\frac{\dot{\bar{\epsilon}}}{\dot{\epsilon}_0}\right]^m \tag{17}$$

where n is the strain hardening exponent and m is the strain-rate sensitivity of the flow stress. K_0 and ϵ_0 are material constants all defined from the results of a uniaxial tension test carried out at a reference strain-rate, $\dot{\epsilon}_0$. Material constants are listed in Table 1. It has been shown that the material exhibits isotropy in all directions [17, 24]. One set of cups were made under high frictional condition without a lubricant and the other with low friction using a lubricant. In each set, two cups of different depths were drawn. The process variables are summarized in Table 2 and the actual cup dimensions are listed in Table 3.

The coefficients of friction for both lubricated and dry conditions were determined by a series of separately conducted tests [27]. Circular grids of diameter 1.27 mm (0.05 in.) were electrochemically etched on surfaces of the blank sheet. Figure 7 shows the specimens with the grids. Analytical and experimental radial and hoop strain distributions are compared in Figs. 8(a) and 8(b) for the results obtained under the dry condition. A similar trend is observed for the case of lubricated tests.

The results of a separately conducted experimental grid analysis are also presented [25]. The experiment was done on a Clothes Dryer Inner Door made from Aluminum Killed Drawing Quality (AKDQ) steel sheet with thickness of 0.58 mm (0.023 in.). Material constants and process variables are summarized in Tables 1 and 4, respectively. Only the region around one of the edges of the part which could be approximated as an axisymmetric shape was analyzed. The computed and measured strain distributions are compared in Fig. 9.

General agreement between predicted and measured data is

Table 1 Material constants

Material	K_o MPa (ksi)	ϵ_o	$\dot{\epsilon}_o$	n	m	R
HSS	608.4 (88.23)	0.047	2.78×10^{-4}	0.24	0.0078	1
EIDQ	620.6 (90)	0.19	2.78×10^{-4}	0.5	0.0067	1
AKDQ	551.6 (80)	0.15	2.78×10^{-4}	0.48	0.0077	2.2

Table 2 Process variables

Test Condition	Coefficient of Friction	Forming speed mm/s (in/s)	Clamping force N (lb)	Punch load N (lb)	Punch dia. mm (in)	Die opening dia. mm (in)	Punch profile radius mm (in)	Die profile radius mm (in)
Dry	Punch 0.5 Die 0.1 Flange 0.4	1.2 (0.046)	10000 (2250)	24000 (5400)	30.7 (1.21)	36.58 (1.44)	4.83 (0.19)	12.7 (0.5)
Lubricated	Punch 0.12 Die 0.07 Flange 0.005	1.2 (0.046)	10000 (2250)	25800 (5800)	30.7 (1.21)	36.58 (1.44)	4.83 (0.19)	12.7 (0.5)

Table 3 Specifications of cup specimens

Specimen	Cup depth mm (in)	Flange outer dia. mm (in)	Blank dia. mm (in)		Test condition
			Actual	Calculated	
a	7.32 (0.288)	78.50 (3.09)	80 (3.15)	77.40 (3.05)	Lubricated
b	12.52 (0.493)	77.01 (3.03)	80 (3.15)	81.99 (3.23)	
c	5.31 (0.209)	68.28 (2.69)	70 (2.76)	73.36 (2.89)	Dry
d	11.10 (0.437)	65.02 (2.56)	70 (2.76)	70.61 (2.78)	

Table 4 Process variables for dryer door

Forming speed mm/s (in/s)	Clamping force N (lb)	Punch load N (lb)	Punch profile radius mm (in)	Die profile radius mm (in)
218.4 (8.6)	400084 (89947)	211724–229517 (47600–51600)	17.78 (0.7)	11.18 (0.44)

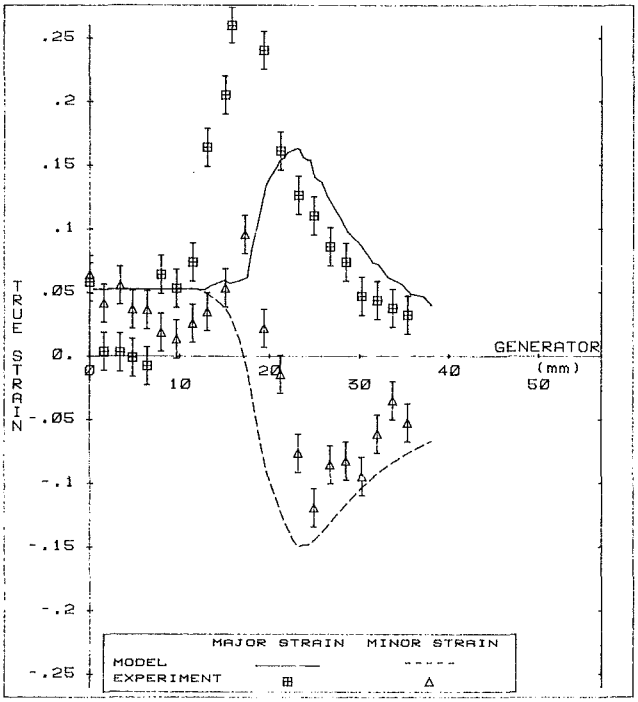

(b)

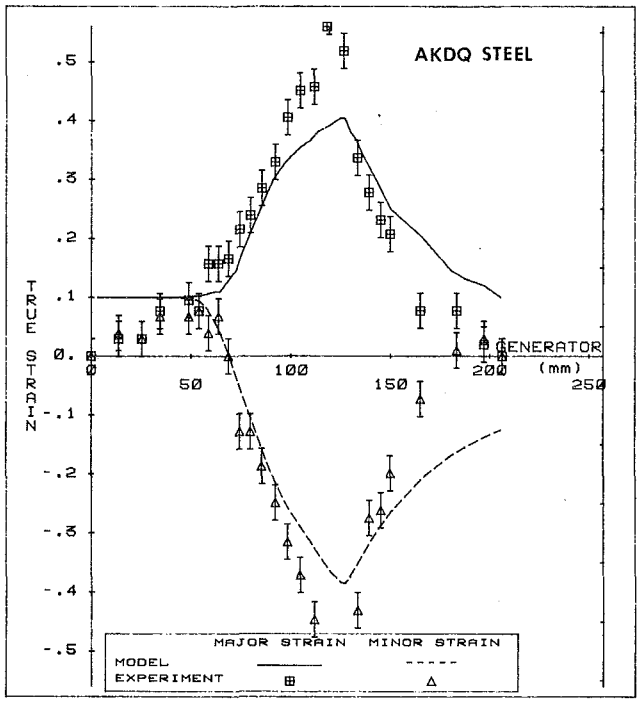

Fig. 9 A comparison of computed major and minor strains along the final generator with experimental data of AKDQ steel dryer door

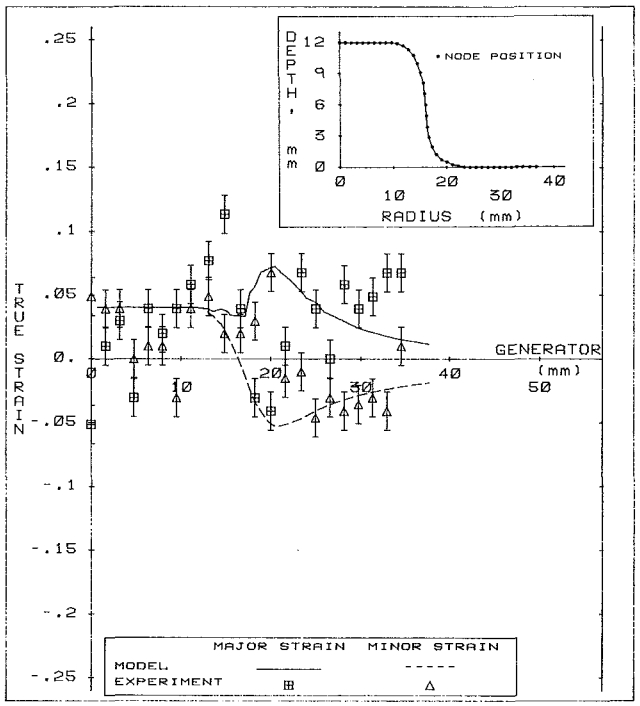

(a)

Fig. 8 A comparison of the computed major and minor strains along the final generator with experimental data of (a) 5.31 mm deep and, (b) 11.10 mm deep cup, made in dry condition. Inset of (a) shows geometry of the formed cup.

observed in all cases. The major discrepancy observed is in the punch profile area where the measured data exceed those predicted by the model. It is worth noting that the predicted constant values of strain components in the flat portion of the punch is a consequence of the assumption of zero frictional force in that region. There is good agreement between actual and predicted blank diameter (Table 3) where the discrepancies are less than 5 percent.

Some of the major sources of error which have been introduced into the analysis and possibly contributed to the discrepancies observed between predicted and measured data are as follows: (1) the fact that the history dependence of plastic deformation is ignored by using total strain theory may cause errors in those regions of the part where strain components are not proportional; (2) errors are introduced when stress and strain are expressed as linear functions of increments, u. Linear approximation of the strain energy may also introduce errors unless a sufficiently small increment of strain is used; (3) the bending and unbending of the material over the die profile is neglected. This simplification has been made in the majority of the analyses, and it is well known that the extra straining of the material due to bending and unbending causes the failure location to be situated closer to the punch profile; (4) there is an uncertainty about the distribution of the coefficient of friction at the metal-tool interfaces.

4 Summary and Conclusions

Some of the numerical enhancements introduced to the original model for one-step forming finite element analysis method were described. Magnitudes and directions of the frictional forces at the metal-tool interfaces have been determined and incorporated into the analysis. The model exhibits cosiderable sensitivity to the coefficient of friction in the punch area. On the other hand, friction at the die-metal interface does not markedly affect the strain distribution. Assignment of friction to the outer rim of the blank holder does not have appreciable effect on the maximum value of tangential strain but increases both tangential and hoop strain in the punch region. In all cases, strain distributions in the punch area and upper portion of the wall section are far more affected by friction than other segments of the cup.

The application of the deformation theory of plasticity in this analysis may contribute some errors, and the effect of

loading history has to be further examined. Moreover, the severity of nonproportionality of strain should also be determined. Such a study has been made in a separate paper [28].

It should be noted that the volume integration of equation (6) is carried out over the initial (undeformed) configuration of the cup, whereas calculations of frictional forces are based on the equilibrium of forces in the final (deformed) geometry. This inconsistency may cause errors at large strain. Dividing the deformation path into several consecutive small steps seems to be a solution to this problem and is discussed in the separate paper [28].

5 Acknowledgments

The authors wish to thank Dr. A. Agah-Tehrani and Dr. A. Kaveh-Ahangar for their valuable comments and discussions. The experimental work was carried out at General Electric Major Appliances Process and Technology Laboratories in Louisville, Kentucky. This research was supported by General Electric Corporate Research and Development.

References

1 Chung, S. Y., and Swift, H. W., "Cup-drawing from a Flat Blank," *Proc. Instn. Mech. Engrs.*, London, Vol. 165, 1951, pp. 199–223.

2 Hill, R., *Mathematical Theory of Plasticity*, Clarendon Press, Oxford, 1950.

3 Woo, D. M., "The Analysis of Axisymmetric Forming of Sheet Metal and the Hydrostatic Bulging Process," *Int. J. Mech. Sci.*, Vol. 6, 1964, pp. 303–317.

4 Woo, D. M., "The Stretch Forming Test," *Engineer*, London, Vol. 220, 1965, pp. 876–880.

5 Woo, D. M., "Analysis of the Cup-drawing Process," *J. Mech. Engng. Sci.*, Vol. 6, 1964, pp. 116–131.

6 Woo, D. M., "On the Complete Solution of the Deep-drawing Problem," *Int. J. Mech. Sci.*, Vol. 10, 1968, pp. 83–94.

7 Yamada, Y., "Studies on Formability of Sheet Metals," Report of the Inst. Ind. Sci., Univ. of Tokyo, Vol. 11, No. 5, 1961.

8 Budiansky, B., and Wang, N. M., "On the Swift Cup Test," *J. of Mech. and Phys. of Solids*, Vol. 14, 1966, pp. 357–374.

9 Lee, C. H., and Kobayashi, S., "New Solutions to Rigid-Plastic Deformation Problems Using a Matrix Method," ASME JOURNAL OF ENGINEERING FOR INDUSTRY, Vol. 95, 1973, pp. 865–873.

10 Kobayashi, S., and Kim, J. H., "Deformation Analysis of Axisymmetric Sheet Metal Forming Processes by the Rigid-Plastic Finite Element Method," *Mechanics of Sheet Metal Forming-Material Behavior and Deformation Analysis*, Plenum Press, New York, 1978, pp. 341–365.

11 Toh, C. H., "Process Modeling of Sheet Metal Forming of General Shapes by the Finite-Element Method Based on Large Strain Formulation," Ph.D. dissertation, Dept. of Mech. Eng., Univ. of Calif., Berkeley, Sept. 1983.

12 Toh, C. H., and Kobayashi, S., "Finite-Element Process Modeling of Sheet Metal Forming of General Shapes," *Fundamentals of Metal Forming Technique—States and Trend, Proc. Int. Symp.*, Oct. 13–14, 1983, Stuttgart, West Germany, pp. 39–56.

13 Kobayashi, S., "Deformation Analysis and Blank Design in Square Cup Drawing," *Advanced Systems for Manufacturing, 12th Conference on Production Research and Technology*, Conference Proceedings, National Science Foundation, Univ. of Wisconsin-Madison, May 14–17, 1985, pp. 258–294.

14 Kim, Y. J., and Yang, D. Y., "A Rigid-Plastic Finite Element Formulation Considering the Effect of Geometric Change and its Application to Hydrostatic Bulging," *Int. J. Mech. Sci.*, Vol. 27, 1985, pp. 453–463.

15 Wifi, A. S., "An Incremental Complete Solution of the Stretch-Forming and Deep-Drawing of a Circular Blank using a Hemispherical Punch," *Int. J. Mech. Sci.*, Vol. 18, 1976, pp. 23–31.

16 Wang, N. M., and Budiansky, B., "Analysis of Sheet Stamping by a Finite-Element Method," ASME *Journal of Applied Mechanics*, Vol. 103, 1978, pp. 73–82.

17 Levy, S., Shih, C. F., Wilkinson, J. P. D., Stine, P., and McWilson, R. C., "Analysis of Sheet Metal Forming to Axisymmetric Shapes," Formability Topics – Metallic Materials, ASTM STP 647, B. A. Niemeier, A. K. Schmieder, and J. R. Newby, eds., 1978, pp. 238–260.

18 Kaftanoglu, B., and Tekkaya, A. E., "Complete Numerical Solution of the Axisymmetric Deep-Drawing Problem," ASME *Journal of Engineering Materials and Technolgy*, Vol. 103, 1981, pp. 326–332.

19 Gerdeen, J. C., "An Analysis of Axisymmetric Sheet Metal Forming," *Proc. NAMRC-II*, Univ. of Wisconsin-Madison, May 1974, pp. 350–365.

20 Gerdeen, J. C., and Soper, D. J., "Computer Simulation of Sheet Metal Forming," SAE Technical Paper 851502, International Off-Highway and Powerplant Congress and Exposition, Milwaukee, Wisconsin, Sept. 9–12, 1985.

21 Oh, S. I., and Rebelo, N., and Kobayashi, S., "Finite Element Formulation for the Analysis of Plastic Deformation of Rate-Sensitive Materials for Metal Forming," *Metal Forming Plasticity, IUTAM Symposium*, Tutzing, Germany, 1978, pp. 273–291.

22 Oh, S. I., and Lahoti, G. D., and Altan, T., "ALPID:A General Purpose FEM Program for Metal Forming," *Proc. NAMRC-IX*, 1981, pp. 83–88.

23 Bathe, K., "*ADINA: A Finite Element Program for Automatic Dynamic Incremental Nonlinear Analysis*, MIT, Cambridge, MA, Dec. 1978.

24 Lee, D., "Computer-Aided Control of Sheet Metal Forming Process," *Journal of Metals*, Vol. 34, 1982, pp. 20–29.

25 Lee, D., and Forth, C. M., "Development of a Computer-Aided Analysis Method for Sheet Material Forming Processes," *Innovations in Materials Processing, Proc. of the 30th Sagamore Conf.*, G. Bruggeman and V. Weiss, eds., Plenum Press, 1985, pp. 161–185.

26 Lee, D., and Stine, P. A., "Computer-Aided Prediction of Sheet Metal Manufacturing Processes and Its Experimental Verification," *Fourth International Conference on Mechanical Behavior of Materials*, The Royal Institute of Technology, Stockholm, Sweden, Aug. 1983.

27 Stine, P. A., Seward, R. E., Beyerle, M. T., and Luken P. C., "CAE Sheet Metal Formability Model—Predictive Capability Improved with Experimentally Derived Input Data," *Computer Modeling of Sheet Metal Forming Process; Theory, Verification and Application*, AIME, N. M. Wang and S. C. Tang, eds. Ann Arbor, Michigan, April 1985, pp. 107–120.

28 Majlessi, S. A., and Lee, D., "Development of Multi-Stage Sheet Metal Forming Analysis Method," to be published.

29 Hutchinson, J. W., and Neale, K. W., "Sheet-Necking-II Time-Independent Behavior," DAS M-4, Division of Applied Sciences, Harvard Univ., Cambridge, Mass., Aug. 1977.

30 Stören, S., and Rice, J. R., "Localized Necking in Thin Sheets," *J. of Mech. and Phys. of Solids*, Vol. 23, 1975, pp. 421–441.